CrossMark

Preliminary physics study of the Lead–Bismuth Eutectic spallation target for China Initiative Accelerator-Driven System

Lu Zhang[1,2] · **Yong-Wei Yang**[1] · **Yu-Cui Gao**[1]

Abstract The Lead–Bismuth Eutectic (LBE) spallation target has been considered as one of the two alternatives for the spallation target for China Initiative Accelerator-Driven System. This paper reports the preliminary study on physical feasibility of a U-type LBE target with window. The simulation results based on Monte Carlo transport code MCNPX indicate that the spallation neutron yield is about 2.5 per proton. The maximum spallation neutron flux is observed at about 3 cm below the lowest part of the window. When the LBE target is coupled with the reactor, the reactor neutrons from the fission reaction increased the neutron field significantly. The energy deposition of high-energy protons is the main heat source; the spallation neutrons and reactor neutrons contribute only a small fraction. The maximum energy deposition in the LBE is about 590 W/cm^3 and that in the target window is about 319 W/cm^3. To estimate the lifetime of the target window, we have calculated the radiation damages. The maximum displacement production rate in the target window is about 10 dpa/FPY. The hydrogen and helium production rates generated during normal operation were also evaluated. By analyzing the residual nucleus in the target during the steady operation, we estimated the accumulated quantities of the extreme radioactivity toxicant ^{210}Po in the LBE target loop. The results would be helpful for the evaluation of the target behavior and will be beneficial to the optimization of the target design work of the experimental facilities.

Keywords LBE spallation target · Target behavior in subcritical reactor · Neutron flux · Energy deposition · Radiation damage · ^{210}Po accumulated quantities

1 Introduction

Along with the development of nuclear energy in the world, the disposal of the high-level radioactive wastes (HLW) becomes a key issue. The studies of accelerator-driven subcritical system (ADS) for transmutation of HLW have been presented in many countries, since the intense spallation neutron source is suitable for transmutation of HLW and the inherent safety of the subcritical system is likely to be accepted by the public [1]. The China Initiative Accelerator-Driven System (CIADS) led by the Chinese Academic of Sciences (CAS) proposed its objective in the first phase: the proton energy is 250 MeV, the maximum beam current is about 10 mA, and the reactor power will reach about 10 MW$_{th}$ [2].

The spallation target for ADS has to endure high energy deposition, so it should have efficient heat removal abilities. Furthermore, using the spallation target-coupled subcritical reactor requires excellent mechanical properties. There are two main choices for the ADS spallation target: one is the solid target consists with rods or plates to produce neutrons and coolant flowing around the elements to

✉ Yong-Wei Yang
yangyongwei@impcas.ac.cn

1 Department of Spallation Target, Institute of Modern Physics, Chinese Academy of Sciences, 509 Nanchang Road, Lanzhou 730000, China

2 University of Chinese Academy of Sciences, Beijing 100049, China

removal the heat, the other is liquid target where the liquid metal acts both as spallation materials and coolant. Solid target can confine the radioactive products efficiently, but its heat-transfer capability is poor and is difficult to couple with the reactor [3]. The liquid target is thought to be the most feasible target because of its good performance on the neutronics and the thermal-hydraulics, and was chosen to be the main target in Europe and Japan [4], but it requires more studies to cope with the radiation damage on the window and the radioactive spallation products. In CIADS, we have two options. One is an innovative granular target that can overcome the heat transfer defects by transporting the target material out the irradiation zone and cooled by a heat exchanger. But, it needs more studies on the behavior when coupled with the reactor. The other is liquid spallation target that is more practicable in the engineering. The U-type casing LBE spallation target studied in this paper is one of the liquid spallation target proposals.

In views of the good performance on the neutronics and the thermal-hydraulics, referring to the successful application in the MEGAPIE [5], we chose the Lead–Bismuth Eutectic (LBE) as the spallation material and coolant for the target. Considering the uncertainty for the stability of the free liquid surface in windowless target [6], a hemispherical shell target window was adopted for the preliminary design. The ferritic and martensitic stainless steel T91 was chosen as the structure material because of its good resistance to creep and swelling under irradiation [7]. To replace the target conveniently, the target was designed as a U-type casing, which could be taken out from the top of the subcritical system easily.

In the ADS system, the proton beam with high current intensity and high energy produced by the accelerator impinges on the spallation target and generates neutrons by nuclear reactions, which are used to drive the subcritical reactor. The spallation neutron yield in leaving the target was obtained by simulation a bare target. By coupling the LBE spallation target with the subcritical reactor CLEAR-I [8], which was designed by the Institute of Nuclear Safety Technology in Chinese Academy of Science (INEST, CAS), the power amplification factor of the subcritical system was obtained, and the required beam current intensity were derived to drive the reactor with a thermal power of 10 MW. Based on the simulation, we obtained the spatial distribution of the energy deposition in the window and the target zone, which gave the main heat sources for thermal hydraulic analysis. Preliminary calculations of radiation damage in the target window were done; the accumulated displacement production rate and helium production rate we obtained are the basic parameters for the target lifetime evaluation. For a LBE spallation target in operation, the leakage of the extreme radioactivity toxicant ^{210}Po would increase the risk of internal exposure.

The calculated spallation product yield and long-term accumulated quantities of ^{210}Po gave basic parameters for the design of the LBE purifier and the LBE loop. These analyses provide the key parameters for the evaluation of the target behavior and would contribute to the optimization of the target design work and the engineering construction.

2 Methodology of simulation

Monte Carlo N-Particle eXtended (MCNPX) transport code [9] developed at Los Alamos National Laboratory has been used for the ADS simulations because of the comprehensive calculation capabilities and the high reliabilities in both the charged particles transport processes and the neutron–photon transport processes. In the high-energy charged particles transport processes, the models of Bertini, Isabel, and INCL4 are used widely as the intranuclear cascade model, while the Dresner and ABLA are used as the evaporation models, which usually combined with the different fission models. There is also a CEM03 [10] model which consists intranuclear cascade model, pre-equilibrium model, and evaporation model. The evaporation and fission/fragmentation processes are handled by the generalized evaporation/fission model. To evaluate these models, an experiment with the 250 MeV proton on the Pb target has been performed at Heavy Ion Research Facility in Lanzhou (HIRFL) [11]. The simulation results of neutron yields using CEM03 model are in good agreement with the experimental results. In addition, the experimental results from other groups in helium product yields [12] and spallation product yields [13, 14] have also strongly supported the simulation results with CEM03 model. Thus, the CEM03 model have been selected for the spallation neutron calculation, the coupled subcritical system analysis, radiation damage analysis, and the spallation production estimations in this work. Furthermore, neutron cross sections based on the ENDF/B-VII.0 data library [15] have been adopted in our simulations.

3 Model of simulation

3.1 Model of spallation target

The preliminary structure of the U-type LBE spallation target with window is shown in Fig. 1. The hemispherical window of the target has an inner radius of 7.4 cm and an outer radius of 7.6 cm. The proton beam from the accelerator penetrates the window and interacts with the LBE in the target zone. A guide tube divides the target zone into two parts, the outer flow channel and the inner flow
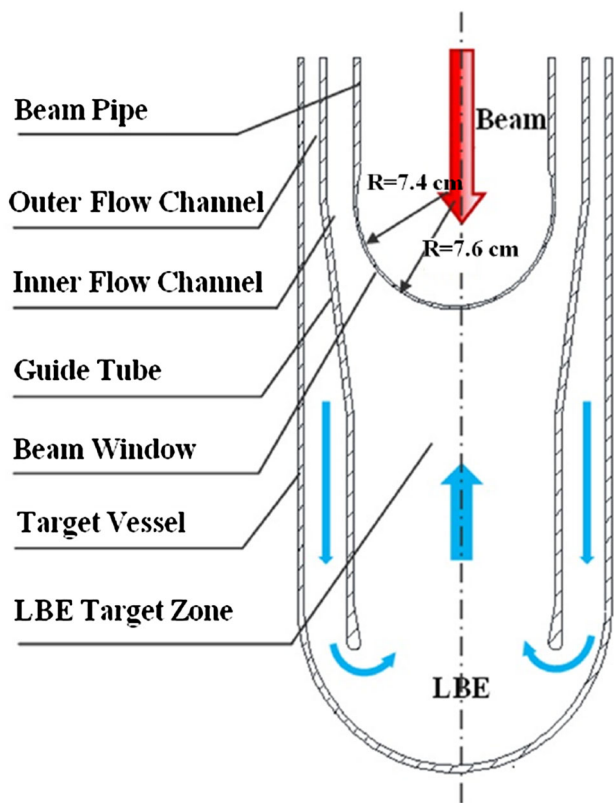
Fig. 1 An elevation view of the U-type windowed LBE spallation target

channel. The LBE flows downwards in the outer flow channel and reaches the target bottom, and then turns upwards to cool the window. After heated by the proton beams, the LBE flows through the channel between the beam pipe and the guide tube. The thermal–hydraulic analyses and structure mechanic analyses about the U-type LBE spallation target can be found in Ref. [16].

3.2 Model of the subcritical reactor coupled with the LBE target

In order to study the behavior of the LBE target coupled with a subcritical reactor, we consider China Lead-based Research Reactor (CLEAR-I) developed by Institute of Nuclear Energy Safety Technology (INEST), Chinese Academy of Sciences [8]. CLEAR-I reactor is a lead-cooled fast reactor with a compact pool-type structure. CLEAR-I will be built with subcritical and critical dual-mode operation capability for validation of ADS transmutation system. The UO_2 with ^{235}U enrichment of 19.75 % is chosen as the fuel, and the cladding material is austenitic steel. The primary and secondary coolant systems are designed to evacuate a maximum thermal power of $10MW_{th}$.

Figure 2a shows the core layout of the reactor which includes spallation target, fuel assemblies, control rods, reflection assemblies, and shielding assemblies. The spallation target is located at the center of the reactor core, which occupied with seven fuel assemblies. Figure 2b shows a vertical cut view of the reactor core. The star in the center of Fig. 2b labeled as "target position" is located at the centre of the hemispherical window, while the dashed line labeled as "zero position" is the axial centre of the core. The vertical distance between the target position and zero position is 11.5 cm.

3.3 The reference beam conditions

For the target design and analyses, beam conditions such as the radius and the current density distribution are the key parameters, which determine the heat transfer and the irradiated mechanic performance. Considering the accidental beam position dislocation with a deviation of about 20–30 % of the beam radius in the high-energy beam transport (HEBT) section of the accelerator, we confined the beam size in a circular with 5 cm of radius and left a space about 2.1 cm to the internal surface of the beam pipe. Taking account of the uniformity that the beam expander can reach, we select a Gaussian beam distribution with a full width at half maximum (FWHM) of 5 cm. The peak density is about 0.018 particles/cm^2 p, as is shown in Fig. 3.

4 Results and analysis

Based on the above-mentioned geometrical models and beam conditions, we have performed numerical simulations with MCNPX code. The simulation results about neutron yield, the amplification factor, the beam current intensity, the energy deposition, neutron flux distributions, neutron spectrum, radiation damage, and the accumulated quantities of ^{210}Po will be discussed as follows.

4.1 Neutron yield, amplification factor, and beam intensities

Numerical calculation showed that when the 250 MeV proton interacted with the LBE target, a proton will create 2.471 neutrons, among which 0.009 neutrons were absorbed by the target material and 2.462 neutrons escaped from the target into the subcritical reactor.

We defined η as the power amplification factor that can be calculated using Eq. (1).

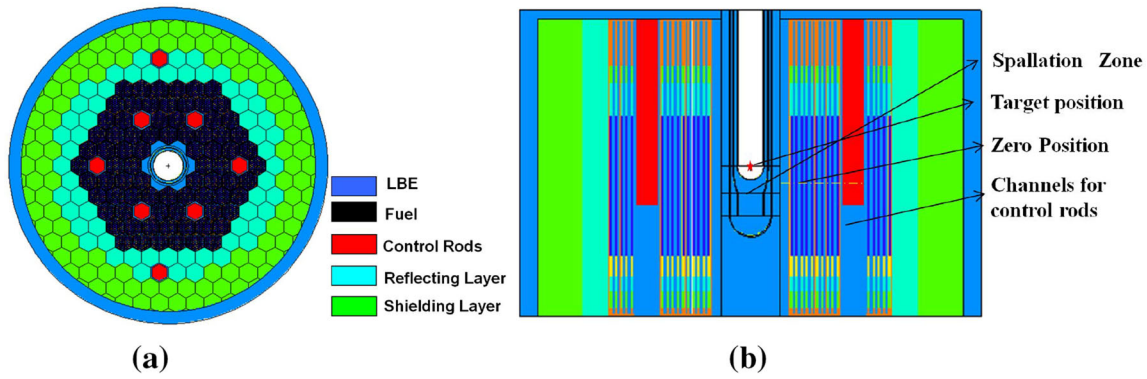$$\eta = \frac{\Psi_p \cdot E_f}{E_p} = \frac{P_r}{P_s} \tag{1}$$

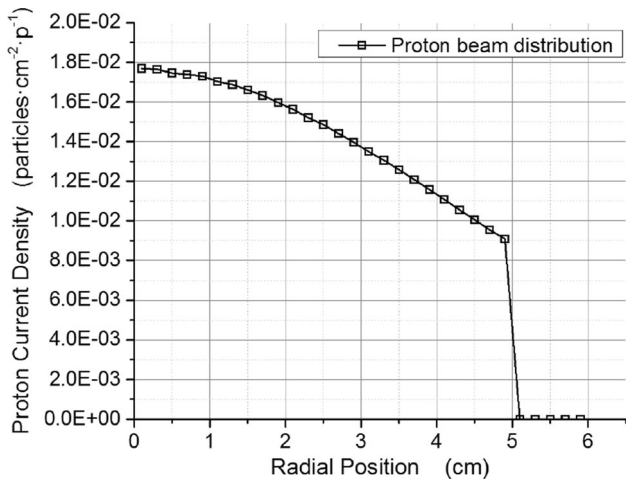Fig. 2 Core layout of the reactor. **a** A top view, **b** a vertical cut view

Fig. 3 Radial distributions of normalized beam intensities on the window

Fig. 4 Energy deposition in the LBE as a function of vertical position during spallation processes

where P_r is the fission power of the subcritical reactor, P_s is the proton beam power, E_p is the proton energy, E_f is the energy released per fission, and the Ψ_p is the number of fissions induced by a proton in the ADS system. For our case, E_f is chosen as 200 MeV, and the Ψ_p was calculated as 68.81 for the system with a K_{eff} of 0.98, and we got the value of η as 53.5. Considering the P_r is 10 MW, the P_s is required to be 0.187 MW, corresponding to a proton beam current intensity of about 0.748 mA.

4.2 Energy deposition in the target and the window

Due to the high energy deposition during the spallation processes, one of the challenges in the design of spallation targets is how to remove heat effectively. For the proton with incident power about 0.187 MW, the energy deposition in the center of the window is nearly 300 W/cm^3. The axial distribution of energy deposition in the target center is similar with the Bragg Curve, and the total range in LBE is about 8 cm. Figure 4 shows the distribution of energy
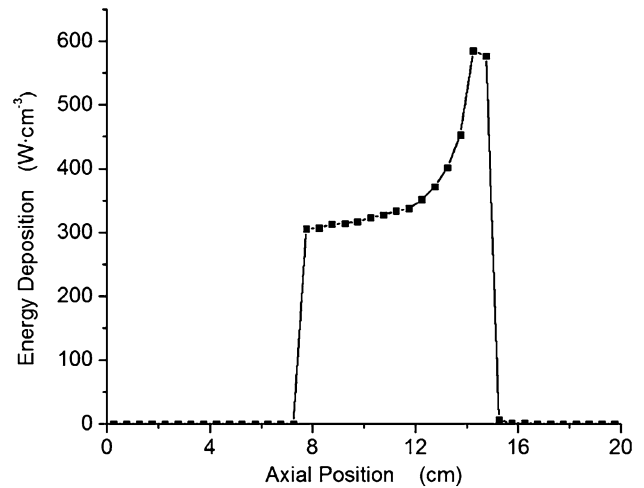
deposition in the LBE as a function of vertical position from the target vessel centerline. For the first 4 cm after interacted with the target, the energy deposition increases slightly, and then, for the second 4 cm, it increases rapidly and reaches the peak at the terminal, about 590 W/cm^3.

The energy deposition in the LBE and the window during the spallation process can be seen from the two-dimensional map shown in Fig. 5. On account of the scattering processes, the energy deposition in the LBE zone exhibits a slightly divergent distribution. As shown in Fig. 5a, the majority of the energy deposition in the LBE lies in the region below the window, from the window bottom down to 8 cm below the window. The energy deposition in other components such as the inner wall, the outer wall, and the beam pipe are negligible. Figure 5b shows the energy deposition in the window during the spallation processes. For the window, the energy deposition comes mainly from the region irradiated by the proton beams. The maximum energy deposition with a value of 314 W/cm^3 is observed at the window bottom. In the region of window without proton irradiation, the energy

Fig. 5 Two-dimensional map of energy deposition in the target (**a**) and window (**b**) during the spallation processes. The numbers from 90 to 270 indicate the angles
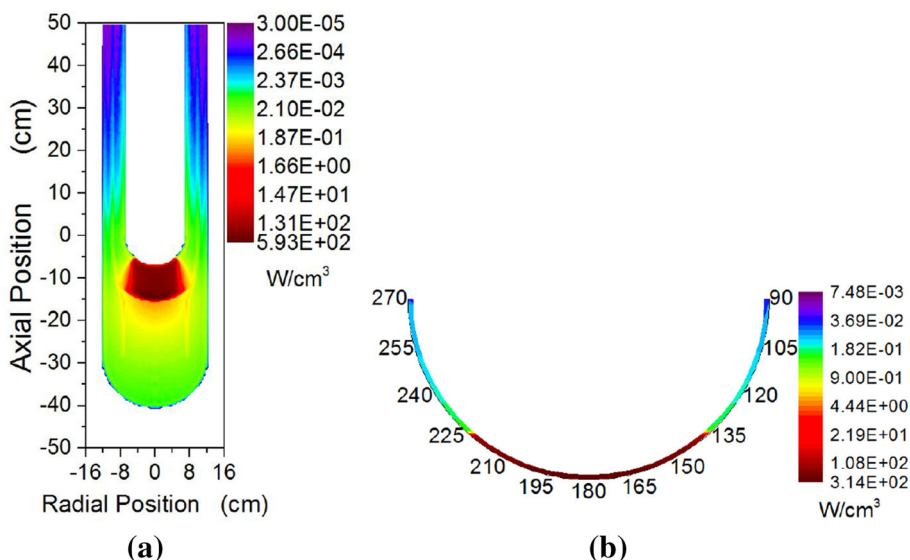
deposition from the secondary spallation particles are about one thousandth of that in the irradiation region.

Figure 6 shows the energy deposition in the LBE and the window when the LBE spallation target is coupled with the CLEAR-I reactor. When the spallation target is coupled with a subcritical reactor, the neutrons come from both spallation process in the spallation target and fission process in the reactor. In the LBE, which has small absorbing and scattering cross section for reactor neutrons, the increase in the energy deposition can be neglected. Figure 6a shows the energy deposition of neutrons in the LBE target. In comparison with the energy deposition of spallation neutrons, the total energy deposition of both spallation neutrons and fission neutrons in the components such as the target window, beam pipe, guide tube, and the vessel increases dramatically, since many fission neutrons from the subcritical reactor enter into these components. On the other hand, the total energy deposition in the LBE target almost keeps unchanged, because the energy deposition due to high-energy protons in the LBE target dominates and the energy deposition of fission neutrons are negligible.

4.3 Neutronic parameters

The flux distribution of spallation neutrons which means all the neutrons generated during the protons interacted with spallation target was simulated. Figure 7a shows the two-dimension distribution of the spallation neutrons flux (SNF) in the target. Almost all the spallation neutrons were generated within the region that irradiated by the proton. The maximum flux is observed at about 3 cm below the lowest part of the window. The flux decreases dramatically

Fig. 6 Two-dimensional heat map of the energy disposition in the target (**a**) and window (**b**) for the coupled system
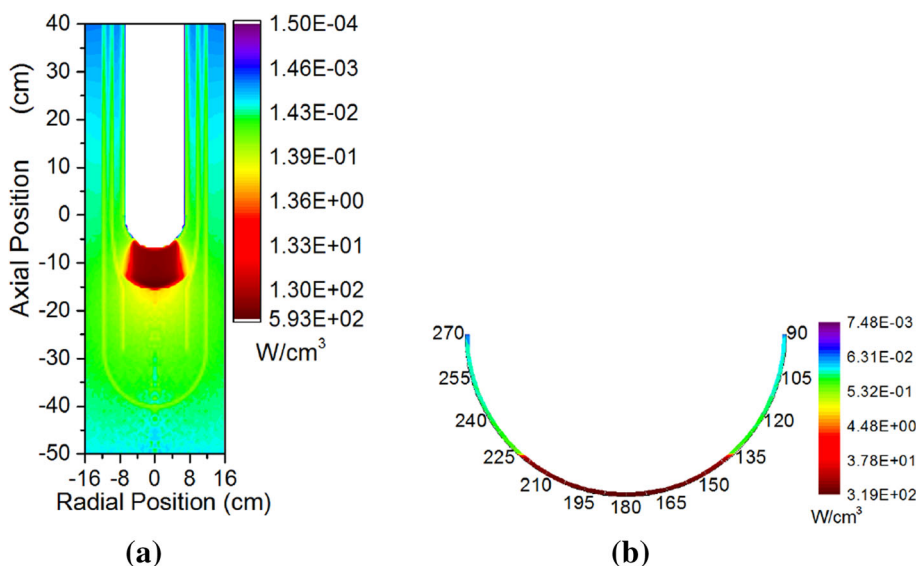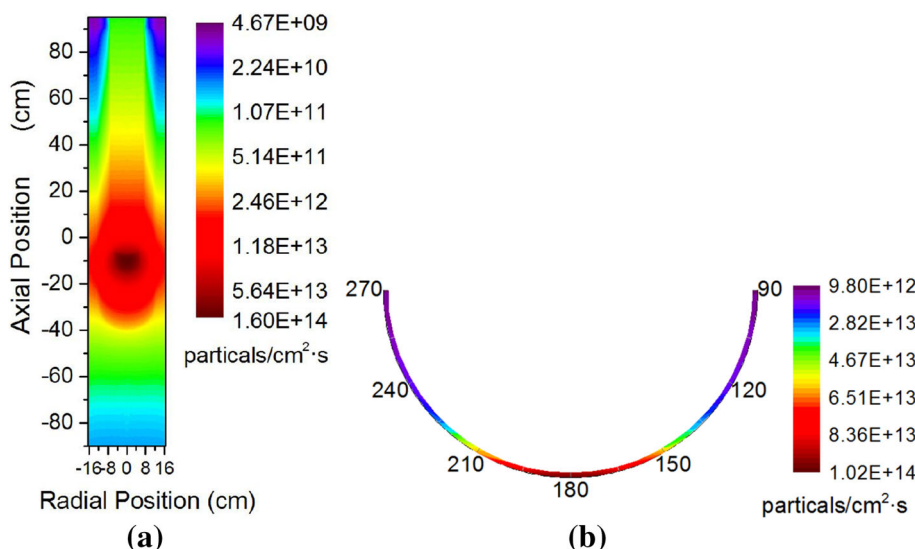
Fig. 7 Two-dimensional distributions of the SNF in the target (**a**) and window (**b**) for the spallation neutrons

with the vertical distance from the window. Since the beam pipe is in the vacuum environment, the SNF is higher than other region at the same axial position that filled with LBE or T91. At the cylindrical surface that is about 16.5 cm from the center axis, the maximum value occurred at the position about 11.5 cm below the target position defined in Fig. 2, which indicated the optimal position of the target in the subcritical system to get a large amplification factor. Figure 7b shows the SNF distribution in the target window. The maximum SNF with a value of about 1.02×10^{14} particles/cm^2 s is observed at the center of the window. The SNF decreases to about 9.8×10^{12} particles/cm^2 s at the edge of the window.

When the LBE target is coupled with the reactor, the fission neutrons from the reactor pass through the target vessel and enter into the target. Compared to that without reactor, more than 1.17×10^{14} particles/cm^2 s neutron flux are added everywhere on the window. The comparison of the neutron field at the window is shown in Fig. 8.

A comparison of the neutron differential spectrum in the cylindrical side wall that is about 16.5 cm from the target center axis is given in Fig. 9, where the NNF means normalized neutron flux. For the spallation neutrons, the highest energy can reach about 250 MeV, and the average energy is about 4.09 MeV. For the coupled system, as the reactor neutrons entered, the fraction of the neutrons below 10 MeV increased significantly, in consequence, the average energy is lowered to about 0.4 MeV.

4.4 Radiation damage

In an ADS system, the target is bombarded by an intensive proton beam. A critical challenge in the design of target window is about the radiation damage caused by these high-energy protons, the spallation neutrons, and the fission
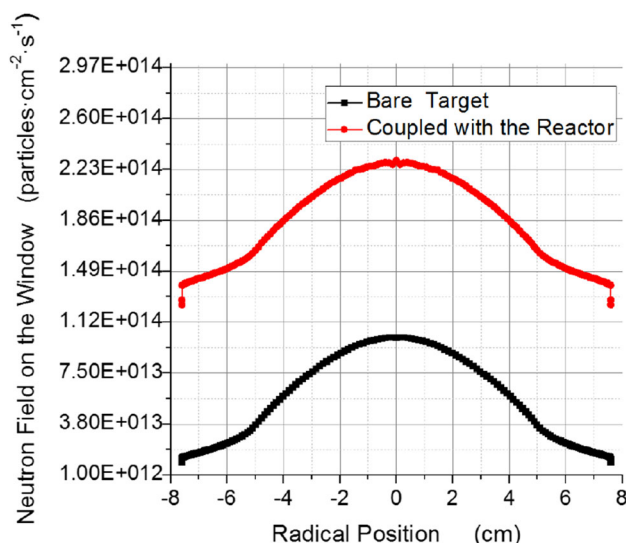
Fig. 8 Comparison of the Neutron field on the window for the spallation neutrons (*black*) and the neutron field that coupled system (*red*). (Color figure online)

neutrons. In this subsection, we evaluate the displacement and the gas production rate, due to which the mechanic property of the window will deteriorate significantly.

In the displacement production rate calculation, we used the neutron and proton cross sections of T91 [17] ranging to 3 GeV given by NRT standard [18]. The displacement production rates (DPR) were evaluated in the time scale of one full power year (FPY), or 24 h each day and a year of 365 days operation. The DPR distribution caused by the proton is similar to the proton intensities distribution as the high-energy proton about 250 MeV is dominant in the window, the maximum value at the center of window is 6.53 dpa/FPY under the peak current about 12.5 μA/cm^2. The maximum DPR caused by the spallation neutrons is about
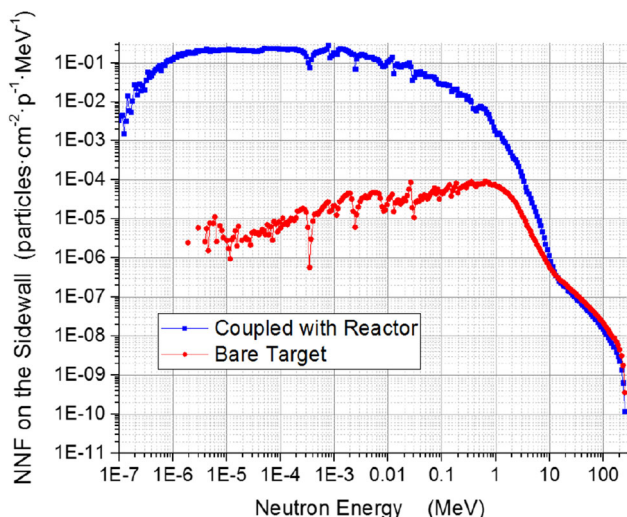
Fig. 9 Comparison of the neutron differential spectrum on the sidewall for the spallation processes and the neutrons for coupled system

Fig. 11 Radial distributions of hydrogen production rate on the target window

3.08 dpa/FPY. Although about 1.17×10^{14} particles/cm^2 s neutron flux were added in the window by the reactor neutrons, the DPR produced by the reactor neutrons is about 0.96 dpa/FPY mA on the window. The blue curve line in Fig. 10 shows the total DPR distribution caused by the spallation processes on the window; in this case, the maximum value is about 9.61 dpa/FPY in the center. The green curve line give the total DPR distribution on the window when the target is coupled with the reactor; here, the maximum occurred in the center is about 10.57 dpa/FPY.

During the irradiation, the light gas such as hydrogen and helium accumulated in the structure material would induce the embrittlement. The gas production can be used to estimate the radiation damage. From Figs. 11 and 12, we can obtain the radial distributions of total hydrogen and
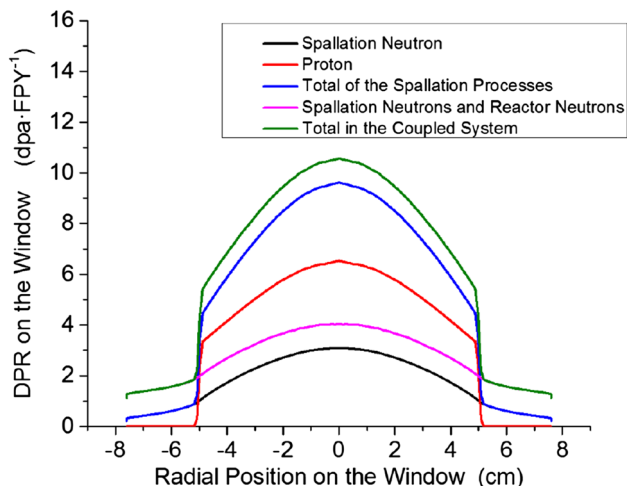

Fig. 12 Radial distributions of helium production rate on the target window

helium in the window; the distributions of this two gases are slightly different in the center of the window. The maximum GPR of these two gases are 3064.7 appm/FPY and 526.6 appm/FPY, respectively. Although the hydrogen has a high production rate, but it diffuses rapidly [19], which means even if it is kept inside the material, it is not necessary trapped where it is produced due to the temperature change.

4.5 Spallation products and ^{210}Po production

Many nuclides are produced during the spallation reactions. For the spallation products distribution of the

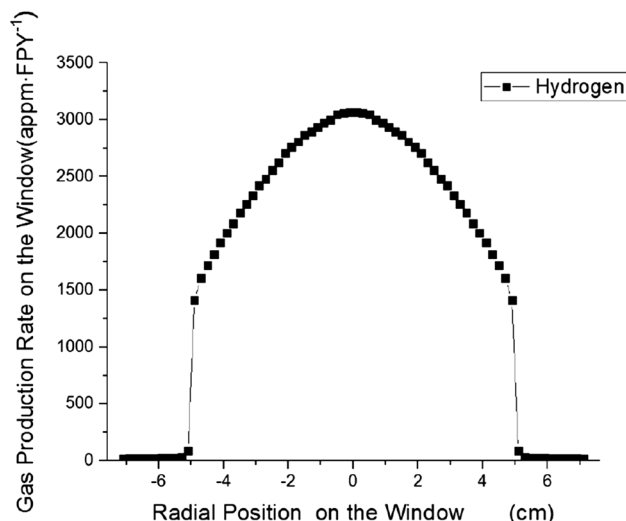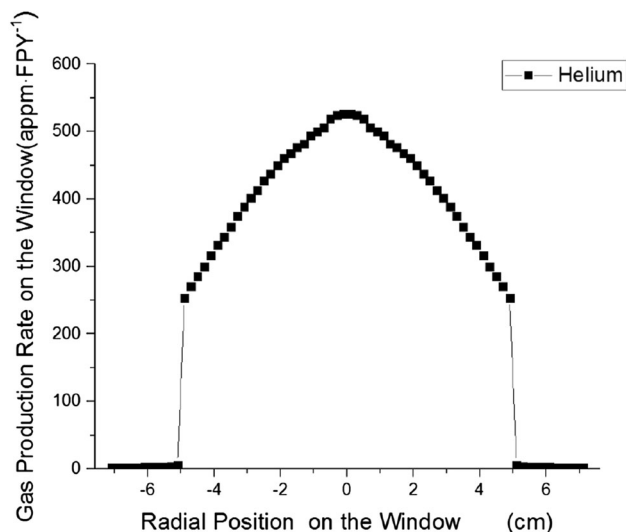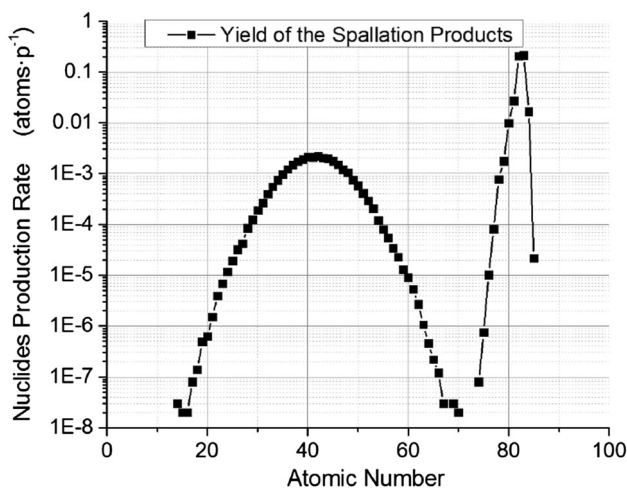Fig. 10 Radial distributions of the displacement production rates on the target window caused by different sources

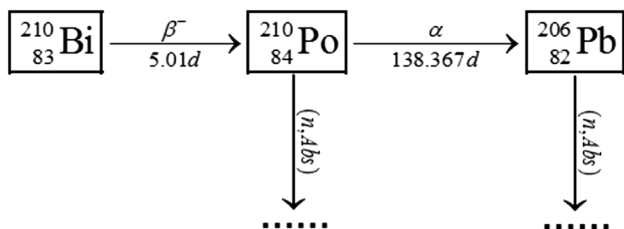**Fig. 13** Atomic number distribution of the spallation products yield

Fig. 14 Main reaction chain of ^{210}Po

LBE target, there are two peaks, one is a spallation–evaporation peak around the atomic number of 82, and the other is a spallation–fission peak around the atomic number of 40, as shown in Fig. 13. The total amount of fission products is about 5.6 % of all that induced by the all the spallation reactions. We can assume that there are two fission debris for one fission reaction, so the portion of fission reactions is about 2.8 %.

Some of the spallation products are toxic, especially for the LBE spallation target. ^{210}Po is an isotope with extreme radioactivity toxicity, which will decay by alpha emission with a half life time about 138.4 days. Furthermore, the ^{210}Po in LBE tended to volatilize to form aerosol when interacted with the gases, this would increase the risk of internal exposure [20] under certain cases of the leakage in the LBE loop.

Figure 14 gives the reaction chain of ^{210}Po, where the (n, Abs) stands for the lost item due to the neutron absorption reaction. Estimations of the accumulated ^{210}Po quantities are done based on this reaction chain.

The differential Eq. (2) describes the relationship between ^{210}Po and ^{210}Bi; the deconstructions of the ^{210}Po and ^{210}Bi in the proton irradiation are ignored since low nucleus density of these two nuclides in the proton-irradiated zone. $N_{Po}(t)$ and $N_{Bi}(t)$ stand for the accumulated nuclides' quantities at the time t, λ_{Po} and λ_{Bi} are the decay constants, Y_{Po} and Y_{Bi} are the yields of ^{210}Po and ^{210}Bi normalized to per mA, $\sigma_a^{Po}\phi$ and $\sigma_a^{Bi}\phi$ are the lost items due to the neutron absorption reactions.

$$\begin{cases} N_{Po}(0) = 0; N_{Bi}(0) = 0 \\ \dfrac{\partial N_{Po}(t)}{\partial t} = I_p Y_{Po} + \lambda_{Bi} N_{Bi} - \lambda_{Po} N_{Po} - \sigma_a^{Po}\phi N_{Po} \\ \dfrac{\partial N_{Bi}(t)}{\partial t} = I_p Y_{Bi} - \lambda_{Bi} N_{Bi} - \sigma_a^{Bi}\phi N_{Bi} \end{cases} \quad (2)$$

Using the maximum neutron flux together with the maximum cross sections of the absorption reactions of the ^{210}Bi and ^{210}Po in TENDL [21] which is ranged from 10^{-11} MeV to 200 MeV, evaluations for the lost terms caused by neutron absorption had been done. The results show that the lost items of neutron absorptions are <1 % of the lost items of the decay, so the neutron absorptions of ^{210}Bi and ^{210}Po can be neglected. On account of this conclusion, we got the accumulated nuclides' quantities described in Eq. (3) by solving the Eq. (2).

$$\begin{cases} N_{Bi}(t) = \dfrac{I_p Y_{Bi}}{\lambda_{Bi}}\left(1 - e^{-\lambda_{Bi}\cdot t}\right) \\ N_{Po}(t) = \dfrac{I_p Y_{Bi} + I_p Y_{Po}}{\lambda_{Po}}\left(1 - e^{-\lambda_{Po}\cdot t}\right) + \dfrac{I_p Y_{Bi}}{\lambda_{Po} - \lambda_{Bi}}\left(e^{-\lambda_{Po}\cdot t} - e^{-\lambda_{Bi}\cdot t}\right) \end{cases} \quad (3)$$

Based on the Eq. (3) and the calculated parameters listed in Table 1, we can draw the conclusion that the main source of the ^{210}Po is the beta decay of ^{210}Bi, and the ^{210}Po produced by the spallation reaction is only about 0.01 % of the total amount. Supposing the system is on operation for 60,000 days, we obtained the time-accumulated quantities curve as is shown in Fig. 15. The ^{210}Po increases gradually since the irradiation begins, and after nearly 1000 days, the amount of accumulated ^{210}Po would keep constant. About 6.15×10^{21} atoms are totally produced, of which only 1.82×10^{20} atoms are produced by the proton sources and the spallation neutrons. When the LBE spallation target was coupled with the reactor, approximately 97 % of the ^{210}Po were produced by the reactor neutrons that added to the target loop.

Table 1 Parameters lists for accumulated quantities analyses

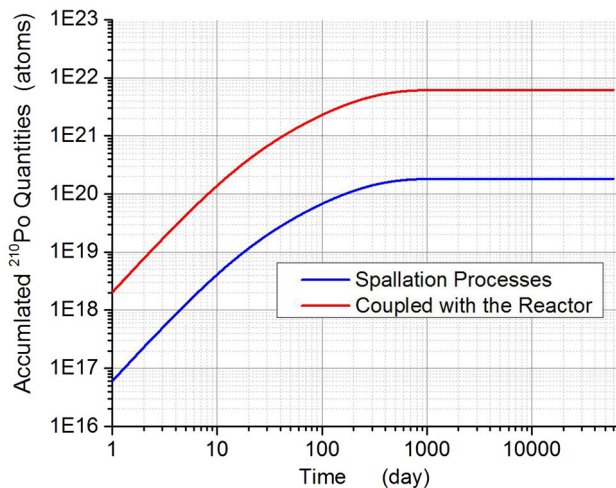| Case	Y_{Bi} (atoms s^{-1})	λ_{Bi} (s^{-1})	Y_{Po} (atoms s^{-1})	λ_{Po} (s^{-1})
Spallation Processes	1.060E13	1.601E−6	1.017E9	5.798E−8
Coupled with CLEAR-I	3.567E14	1.601E−6	1.017E9	5.798E−8

Fig. 15 Temporal distribution of the accumulated ^{210}Po quantities in the target loop for the spallation processes (*blue*) and the coupled case (*red*). (Color figure online)

5 Conclusion

We designed a U-type LBE spallation target with window for the CIADS, which is intended to reach a thermal power of 10 MW for the subcritical reactor driven by 250 MeV protons. About 2.5 spallation neutrons with the average energy of 4.05 MeV leaked out of the spallation target. Analyses showed that when coupled with a subcritical reactor of $k_{eff} = 0.98$, the amplification factor is 53.5. This means the beam current needed for this system is about 0.748 mA. When the subcritical system runs on the steady state, the peak energy deposition in the window and the LBE can reach to about 319 and 590 W/cm^3, respectively. This energy deposition can be easily removal by the LBE loop [16]. The maximum neutron flux in the window is about 2.24×10^{14} n/cm^2 s. The maximum displacement production rate in the window is about 10.57 dpa/FPY, the peak helium production rate is about 526.6 appm/FPY, and the peak hydrogen production rate is about 3064.7 appm/FPY. According to the acceptable radiation damage (15 dpa, 1000 appm helium) suggested by the PSI [22], the target window can serve for more than one full power year, but mechanical analyses concerning the creep, corrosion, and fatigue behavior should be performed for a better estimate of the life time. The ^{210}Po accumulates gradually during the irradiation and reaches the constant quantities about 6.15×10^{21} atoms in the target loop after 1000 days. Such amount of ^{210}Po means we should pay more attention in the future design of the target loop to limit the polonium compound leaking. The spatial distributions of the energy deposition and neutron flux were obtained. The radial distribution of the radiation damage and the time distribution of the accumulated ^{210}Po quantities were also estimated.

The main heating source in the target is due to the protons, and the reactor neutrons contribute very little. More than half the displacement production on the window is induced by the protons, and the spallation neutrons are another main source due to the hard spectrum. Although more than 1.17×10^{14} n/cm^2 s reactor neutrons flux added on everywhere of the window, the displacement production induced by the reactor neutrons is very small since their spectrums is very soft with an average energy about 0.36 MeV. When the 250 MeV protons interact with the LBE target, the fraction of fission reaction is only 2.8 % of all the spallation-induced reactions. The ^{210}Po generated by the spallation reactions is only about 3 % of that induced by the reactor neutrons.

In this article, we presented several aspects of the spallation target, and this work is expected to contribute to the future research and development of CIADS.

References

1. C.D. Bowman, E.D. Arthur, P.W. Lisowski et al., Nuclear energy generation and waste transmutation using an accelerator-driven intense thermal neutron source. Nucl. Instrum. Methods A **320**, 336–367 (1992). doi:10.1016/0168-9002(92)90795-6
2. Z. Wenlong, X. Hushan, Advanced fission energy program-ADS transmutation system. Bull. Chin. Acad. Sci. **27**(3), 375–381 (2012). doi:10.3969/j.issn.1000-3045.2012.03.017
3. H.A. Abderrahim, J. Galambos, Y. Gohar et al., Accelerator and target technology for accelerator driven transmutation and energy production. DOE white paper on ADS, vol. 1, no. 1 (2010), pp. 1–23. http://192.107.175.200/∼/media/hep/pdf/files/pdfs/ADS_White_Paper_final.pdf
4. T. Sugawara, K. Nishihara, H. Obayashi et al., Conceptual design study of beam window for accelerator-driven system. J. Nucl. Sci. Technol. **47**(10), 953–962 (2010). doi:10.1080/18811248.2010.9720974
5. C. Fazio, F. Gröschel, W. Wagner et al., The MEGAPIE-TEST project: supporting research and lessons learned in first-of-a-kind spallation target technology. Nucl. Eng. Des. **238**(6), 1471–1495 (2008). doi:10.1016/j.nucengdes.2007.11.006
6. A. Batta, A. Class, Numerical investigations on geometrical designs of the windowless XT-ADS spallation target, in *International Congress on Advances in Nuclear Power Plants (ICAPP07)*, Nice, France, May. 13–18, 2007
7. J.B. Vogt, A. Verleene, I. Serre et al., Understanding the liquid metal assisted damage sources in the T91 martensitic steel for safer use of ADS. Eng. Fail. Anal. **14**(6), 1185–1193 (2007). doi:10.1016/j.engfailanal.2006.11.075
8. W. Yican, Y. Bai, Y. Song, Q. Huang, Z. Zhao, H. Liqin, Development strategy and conceptual design of China lead-based research reactor. Ann. Nucl. Energy **87**, 511–516 (2016). doi:10.1016/j.anucene.2015.08.015
9. D. Pelowitz, *MCNPX User's Manual 2.7.0* (Los Alamos National Laboratory, Los Alamos, 2011)
10. S.G. Mashnik, A.J. Sierk, K.K. Gudima et al., CEM03 and LAQGSM03—new modeling tools for nuclear applications.

J. Phys: Conf. Ser. **41**(1), 340 (2006). doi:10.1088/1742-6596/41/1/037

11. L. Chen, F. Ma, X.Y. Zhang et al., Spallation yield of neutrons produced in thick lead target bombarded with 250 MeV protons. Nucl. Instrum. Methods B **342**, 87–90 (2015). doi:10.1016/j.nimb.2014.09.020

12. W. Lu, F.X. Gallmeier, P.J. Geoghegan et al., A reevaluation of radiation damage cross sections. J. Nucl. Mater. **431**(1), 33–38 (2012). doi:10.1016/j.jnucmat.2011.12.016

13. M.S. Sabra, R.A. Weller, M.H. Mendenhall et al., Validation of nuclear reaction codes for proton-induced radiation effects: the case for CEM03. IEEE Trans. Nucl. Sci. **58**(6), 3134–3138 (2011). doi:10.1109/TNS.2011.2169989

14. Y.E. Titarenko, V.F. Batyaev, R.D. Mulambetov et al., Excitation functions of product nuclei from 40 to 2600 MeV proton-irradiated 206,207,208, nat Pb and 209 Bi. Nucl. Instrum. Methods A **562**(2), 801–805 (2006). doi:10.1016/j.nima.2006.02.059

15. M.B. Chadwick, P. Obložinský, M. Herman et al., ENDF/B-VII. 0: next generation evaluated nuclear data library for nuclear science and technology. Nucl. Data Sheets **107**(12), 2931–3060 (2006). doi:10.1016/j.nds.2006.11.001

16. D. Fan, Y. Yang, Y. Gao et al. Thermal-hydraulics design of the LBE spallation target system for CIADS, in *23nd International Conference on Nuclear Engineering (ICONE23)*, Chiba, Japan, May. 17–21, 2015

17. Y. Iwamoto, H. Iwamoto, M. Harada et al., Calculation of displacement cross-sections for structural materials in accelerators using PHITS event generator and its applications to radiation damage. J. Nucl. Sci. Technol. **51**(1), 98–107 (2014). doi:10.1080/00223131.2013.851042

18. M.J. Norgett, M.T. Robinson, I.M. Torrens, A proposed method of calculating displacement dose rates. Nucl. Eng. Des. **33**(1), 50–54 (1975). doi:10.1016/0029-5493(75)90035-7

19. Y. Dai, Y. Foucher, M.R. James et al., Neutronics calculation, dosimetry analysis and gas measurements of the first SINQ target irradiation experiment, STIP-I. J. Nucl. Mater. **318**, 167–175 (2003). doi:10.1016/S0022-3115(03)00099-0

20. T. Obara, T. Miura, Y. Fujita et al., Preliminary study of the removal of polonium contamination by neutron-irradiated Lead–Bismuth Eutectic. Ann. Nucl. Energy **30**(4), 497–502 (2003). doi:10.1016/S0306-4549(02)00089-0

21. A.J. Koning, D. Rochman, S. van der Marck et al., TENDL-2014: TALYS-based evaluated nuclear data library. ftp://ftp.nrg.eu/pub/www/talys/tendl2014/tendl2014.html

22. Z. Tong, Y. Dai, The microstructure and tensile properties of ferritic/martensitic steels T91, Eurofer-97 and F82H irradiated up to 20dpa in STIP-III. J. Nucl. Mater. **398**(1), 43–48 (2010). doi:10.1016/j.jnucmat.2011.04.029